PHYSICAL REVIEW D

PARTICLES AND FIELDS

THIRD SERIES, VOLUME 40, NUMBER 11 1 DECEMBER 1989

# Polarization in inclusive $\Lambda$ and $\bar{\Lambda}$ production at large $p_T$

B. Lundberg,* R. Handler, L. Pondrom, M. Sheaff, and C. Wilkinson†
*Physics Department, University of Wisconsin, Madison, Wisconsin 53706*

J. Dworkin,‡ O. E. Overseth, and R. Rameika*
*Physics Department, University of Michigan, Ann Arbor, Michigan 48109*

K. Heller and C. James*
*School of Physics and Astronomy, University of Minnesota, Minneapolis, Minnesota 55455*

A. Beretvas,* P. Cushman,§ T. Devlin, K. B. Luk,** G. B. Thomson, and R. Whitman††
*Department of Physics and Astronomy, Rutgers–The State University of New Jersey, Piscataway, New Jersey 08855-0849*
(Received 2 June 1989)

A study of the inclusive polarization of $\Lambda$ hyperons produced by 400-GeV/$c$ protons incident on nuclear targets has been performed at Fermilab. The polarization **P** of the $\Lambda$ has been mapped over a large range of $x_F$ and $p_T$ to good precision for $p_T$ up to 3.8 GeV/$c$. The magnitude of the polarization at fixed $x_F$ rises with $p_T$ to a plateau at about 1 GeV/$c$, and the size of the plateau increases monotonically with $x_F$. The $\bar{\Lambda}$ were found to be unpolarized for $p_T < 2.4$ GeV/$c$. A target-nucleus dependence for the $\Lambda$ polarization has been observed.

## I. INTRODUCTION

The polarization of hyperons produced by protons is one of the most universal regularities observed in the strong interactions. Inclusive $\Lambda$ polarization has been observed in the range from 12 to 2000 GeV (equivalent proton energy on fixed targets) (Refs. 1–7). Polarization of roughly the same magnitude is observed in the production by protons of every other hyperon in the fundamental baryon octet.[8–14] Attempts to integrate the remarkably large hyperon polarization into fundamental theories of strong interactions (QCD) have not met with outstanding success, possibly because of the low transverse momentum, $p_T$, of the final-state hyperons. This experiment maps the kinematic behavior of the $\Lambda$ polarization and extends it to a region of $p_T$ where hard-scattering effects are significant.

The discovery of $\Lambda$ polarization from 300-GeV/$c$ inclusive proton-nucleon reactions[1,15] played a major role in the development of a successful program of hyperon physics at Fermilab. For a review see Ref. 16. Use of the phenomenon led directly to the measurements of the magnetic moments of the $\Lambda$ (Ref. 17) $\Xi^0$ (Ref. 8), $\Xi^-$ (Ref. 12), $\Sigma^+$ (Refs. 10 and 18), $\Sigma^-$ (Refs. 11, 13, and 14), and $\Omega^-$(Ref. 19) hyperons. A beam of polarized hyperons was used in a study of $\Sigma^-$ $\beta$ decay[20,21] which resolved an outstanding discrepancy between previous data and Cabibbo theory.[22]

To date, the polarization measurements for $\Lambda$ are the most extensive, and a more detailed description of this phenomenon has gradually emerged as data have been added over a wider range of kinematic variables with several production target materials. The initial observation of $\Lambda$ polarization,[1,15] taken at relatively small production angles, covered only low transverse momentum ($p_T \leq 1$ GeV/$c$), and showed a monotonic increase of polarization with $p_T$. It did not cover a sufficiently broad range of Feynman $x$ ($x_F = p_L^*/p_{\max}^*$, the ratio of the c.m. longitudinal momentum to its maximum possible value) at any given $p_T$ to reveal a significant $x_F$ dependence. No statistically significant dependence of polarization on target material was reported.

In subsequent experiments including larger production angles, the $\Lambda$ polarization was measured over the range $0.15 < x_F < 0.8$ and $0.2 < p_T < 1.5$ GeV/$c$ with targets of Be, Cu and Pb targets,[3,23] and with hydrogen.[24] These measurements suggested that the polarization increased with $x_F$ as well as $p_T$ (Ref. 23). From the results of Ref. 24 there was reason to suspect that the polarization flattened above $p_T \approx 1$ GeV/$c$ instead of continuing to grow

 ©1989 The American Physical Society

monotonically. Studies of $\Lambda$ polarization produced on several nuclear targets showed a slightly larger polarization from Be and H than from heavy nuclei such as Cu, W, and Pb (Refs. 6 and 24–26).

Presented here are the results of an experiment which measured the detailed behavior of the inclusive $\Lambda$ polarization with respect to the kinematic variables $x_F$ and $p_T$. A total of $7.6\times10^6$ $\Lambda\to p\pi^-$ reconstructed over the range $0.2<x_F<0.8$ and $0.8<p_T<3.8$ GeV/$c$ were used in the polarization analysis. Results from the present experiment strongly confirm the dependence of the polarization of $x_F$, $p_T$, and target material suggested by previous experiments. (See Sec. V.) The polarization is found to have a remarkably simple behavior which is well described by the product of two factors. One, a function of $p_T$ alone, increases in magnitude monotonically from $p_T=0$ to a plateau at $p_T\approx1$ GeV/$c$. The other, a nearly linear function of $x_F$ alone, extrapolates to zero polarization at $x_F=0$. Also obtained were $0.8\times10^6$ $\bar{\Lambda}\to\bar{p}\pi^+$. These were subjected to a similar study and the polarization was found to be consistent with zero in the region $0.15<x_F<0.29$ and $0.6<p_T<2.3$ GeV/$c$.

## II. APPARATUS AND PROCEDURES

The experiment was performed at Fermilab in the M2 beam line with protons at 400 GeV steered at various angles onto a production target. Since the production of hyperons falls as the production angle increases, the flux of incident protons on target was increased to compensate partially for this effect. Intensities between $10^8$ and $5\times10^{10}$ protons per second were used.

The 400-GeV/$c$ proton beam was transported to the experimental area by a magnetic beam transport system. The directions of the incident proton beam, $\hat{\mathbf{k}}_{\rm in}$, and the outgoing hyperon beam, $\hat{\mathbf{k}}_{\rm out}$, defined the production plane at the production target, with the normal $\hat{\mathbf{n}}=\hat{\mathbf{k}}_{\rm in}\times\hat{\mathbf{k}}_{\rm out}/|\hat{\mathbf{k}}_{\rm in}\times\hat{\mathbf{k}}_{\rm out}|$. The production angle was defined as positive when $\hat{\mathbf{n}}$ pointed vertically upwards.[27] The coordinate system used in this report has the $z$ axis pointing downstream along the centroid of the neutral beam, i.e., $\hat{\mathbf{z}}=\hat{\mathbf{k}}_{\rm out}$, $\hat{\mathbf{y}}$ vertically upward, and $\hat{\mathbf{x}}$ horizontal, completing a right-handed coordinate system.

Production at nonzero angles was controlled by an angle-varying-bend (AVB) system of five 6-m-long dipole magnets, shown in Fig. 1. Each magnet had a maximum field integral of 11 T m. A motorized system was used to displace the magnet string into an arc in the horizontal plane so that angles as large as 25 milliradians (mrad) could be achieved. A precision position encoder was used to ensure reproducibility of the production angle throughout the experiment. The production angle was reversed every few hours to cancel systematic errors. Data were taken at nominal incident angles of $\pm6$, $\pm7$, $\pm10$, $\pm12$, $\pm20$, and $\pm24$ mrad in the $x$-$z$ plane.

With the AVB system off, the proton beam could be steered onto the production target and (with the target removed and M1 field off) through the neutral beam collimator to establish a zero-production-angle reference axis in our detector.

The primary determination of the production angles came from the known field integrals of the AVB magnets and the direction of the neutral beam relative to the zero-production-angle reference axis. The value of the angle for each AVB setting was checked by the measured positions of the beam centroid as it passed through two segmented-wire ion chambers (SWIC's) with 1-mm wire spacing. The SWIC's (not shown in Fig. 1) were placed 4 m apart just upstream of the production target and gave measurements of the production angle to about 0.1 mrad.

Cylindrical targets were mounted in a vertical positioning device, 2 m downstream of the final beam transport element. Virtually all of the polarization data were taken with a beryllium target with a 9.6-mm diameter and a thickness of 15.00 cm, i.e., 0.497 collision lengths ($L_{\rm coll}$). Additional data were taken with 12.6-mm-diameter copper and lead targets with lengths of 4.64 cm$=0.486L_{\rm coll}$ and 4.84 cm $=0.473L_{\rm coll}$, respectively. The target positioning device also included an empty slot for measuring the background from nontarget-produced events.

The neutral hyperon beam was formed by a brass and tungsten collimating channel with a 4-mm-diameter defining aperture located at the midpoint of a 5.3-m-long-magnet, M1. The field in M1 was horizontal with a field integral of 12.0 T m. This deflected the proton beam by 4.8 mm in the $y$-$z$ plane at the entrance to the defining

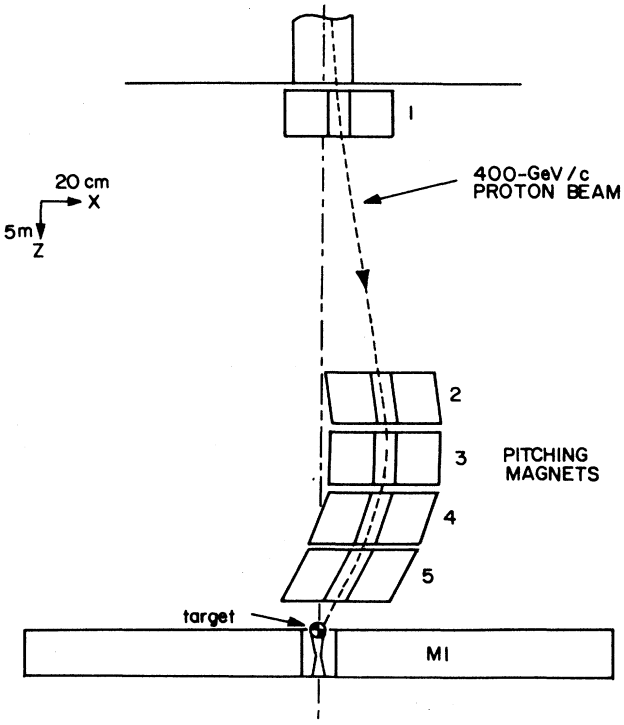


FIG. 1. A system of five Fermilab B1 dipole magnets was designed to transport a 400-GeV/$c$ proton beam to the experimental target at angles $\theta_p$ as large as $\pm25$ mrad.

aperture so that only a neutral beam entered the spectrometer. This magnetic field also precessed the spin vector of the Λ through an angle

$$\phi=(18.30\ \text{deg/T m})(\mu_\Lambda/\mu_N)\int B\,dl\ , \tag{1}$$

where $\mu_\Lambda$ is the magnetic moment of the Λ and $\mu_N$ is the nuclear magneton. The collimator aperture was filled with helium gas to minimize interactions.

The layout of the spectrometer is shown in Fig. 2. It used multiwire proportional chambers (MWPC's) ($C_1$–$C_6$), scintillation counters ($S_1$–$S_2$), and a superconducting dipole analyzing magnet $M_2$. The field in $M_2$ was vertical and had a bending power equivalent to a momentum transfer of 0.95 GeV/$c$. This apparatus has been described extensively elsewhere.[15] Further details specific to this experiment can be found in Ref. 28.

Scintillation counters were used in conjunction with prompt outputs from some of the MWPC's to trigger the data-acquisition electronics. Several triggers were used simultaneously to enhance the collection of high-$p_T$ events and to reduce possible systematic errors in the determination of the spectrometer's acceptance. The least restrictive trigger T1 was a simple "$V$ topology," to recognize the charged decay mode of neutral particles. The requirements for T1 were: a neutral particle entering the evacuated decay region, and both positive and negative decay products emerging from the analysis magnet. Symbolically, T1 is designated by the coincidence of the signals:

$$\text{T1}=\bar{S}_1\cdot S_2\cdot C_{1x}\cdot C_{1y}\cdot C_{5xR}\cdot C_{5xL}\cdot C_{5y}\ , \tag{2}$$

where $x$ ($y$) refers to any vertical (horizontal) wire in the specified chamber, and $R$ ($L$) designates any wire to the right (left) side of a trigger boundary. The trigger boundary in $C_5$ was located at the center of the chamber. This trigger had a high (>90%) efficiency for $\Lambda\to p\pi^-$ with decay vertices between $S_1$ and $S_2$.

A second trigger T2 was designated to favor high-momentum Λ's and to suppress the acceptance for low-momentum Λ's and other particles by selectively triggering on the high-momentum daughter protons which passed through $C_{6xR}$. Since the neutral beam channel accepted particles over the entire momentum range of the production spectrum, and the Λ production spectrum decreases rapidly in $p_T$, without some selectivity in the trigger relatively low momentum Λ's would have saturated the live time of the data-acquisition system. This selectivity was provided by taking fast output signals from two selected groups of vertical wires in $C_6$. (See Fig. 2.) In $C_6$ the boundaries $C_{6xR}$ and $C_{6xL}$ near the beam line were displaced to $x=-2.8$ cm and $x=+2.0$ cm, respectively, to prevent triggers from the charged products of neutral-particle interactions downstream of $M_2$. The other boundaries were chosen to restrict the momentum spectrum.

A third trigger T3 performed a similar function for $\bar{\Lambda}$ using $C_{6xL}$. T3 was not symmetric with T2. Instead, the boundaries of $C_{6xL}$ were chosen to accept $\bar{p}$'s from low momentum $\bar{\Lambda}$'s and to exclude the highest momentum $\pi^-$ from Λ decay. Symbolically,

$$\text{T2}=\text{T1}\cdot C_{6xR} \tag{3}$$

and

$$\text{T3}=\text{T1}\cdot C_{6xL}\ . \tag{4}$$

At 50 GeV, the yield of T2 to T1 triggers was suppressed by a factor of ~50. Above 100 GeV the difference in yield between T1 and T2 triggers was negligible. The final trigger was

$$T=\tfrac{1}{32}\text{T1}+\text{T2}+\tfrac{1}{4}\text{T3}\ , \tag{5}$$

where $\frac{1}{32}$T1 and $\frac{1}{4}$T3 indicate that the raw triggers were prescaled by factors of 32 and 4, respectively.

The overall acceptances of the apparatus for $\Lambda\to p\pi^-$, $\bar{\Lambda}\to\bar{p}\pi^+$, and $K^0_S\to\pi^+\pi^-$ are shown in Fig. 3. The acceptance was defined as the probability that the parent particle decayed between $S_1$ and $C_1$, and that its daughter particles passed through all the spectrometer apertures and satisfied the trigger requirements above (T2 for Λ; T3 for $\bar{\Lambda}$ and $K^0_S$). In principle, the acceptance is a function of all five variables of the neutral beam phase space: the magnitude of the momentum $p$, the transverse position ($x$,$y$) evaluated at some suitable $z$ position along the beam line, and the transverse angles of the momentum vector ($\phi_x$,$\phi_y$). We can ignore $x$ and $y$ because the beam channel collimator was stable in time and nearly pointlike compared to all relevant dimensions of the spectrometer. Since the production angle $\theta_p$ was controlled by steering the proton beam in the horizontal plane, the measured distribution in $\phi_y$ was found to be insensitive to $\theta_p$. Further, the vertical apertures of the spectrometer were fairly far from and symmetric relative to the projected size of the neutral beam. Variation of cuts inside these apertures did not change the results. However, variations in the $\phi_x$ distribution were significant because the trigger boundaries of T2 were fairly close to the projected neutral beam line. This distribution did vary with $\theta_p$ because of the fairly strong $\theta_p$ dependence of the pro-

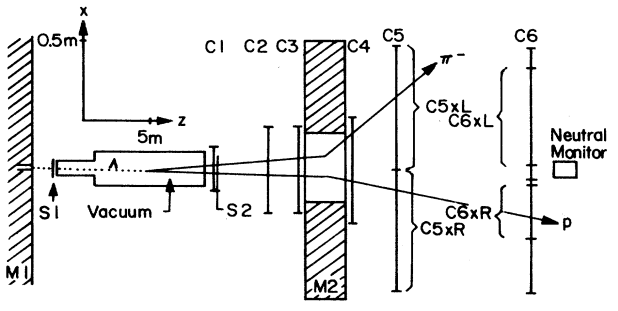


FIG. 2. The plan view of the spectrometer with all relevant detectors and magnets is shown. $C_1$–$C_6$ are multiwire proportional chambers and $S_1$–$S_2$ are scintillation counters. The tracks of a typical high-momentum Λ are also shown. Note that the proton and pion pass through electronically segmented sections of $C_5$ and $C_6$ which are required for a "T2" trigger.

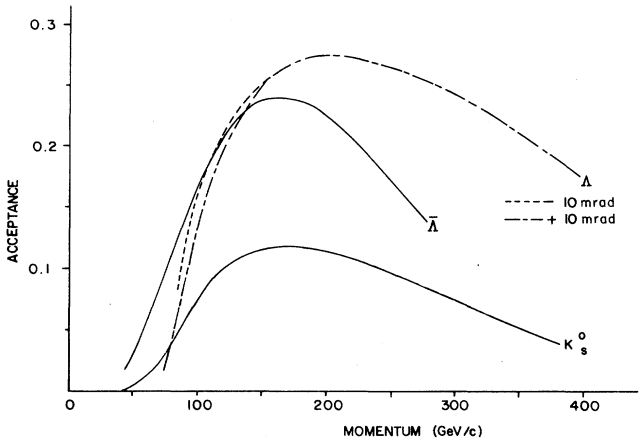


FIG. 3. The acceptance of the apparatus for $\Lambda \to p\pi^-$, $\bar{\Lambda} \to \bar{p}\pi^+$, and $K_S^0 \to \pi^+\pi^-$. The dominant effect is the probability that the particle decays within the fiducial volume. Also included are the geometric efficiency of the spectrometer and triggers boundaries of $\frac{1}{32}$ T1+T2 for $\Lambda$ and T3 for $\bar{\Lambda}$ and $K_0^S$. The variation in acceptance with the sign of the production angle (described in the text) is shown for $\pm 10$ mrad.

duction cross sections, and the fact that the angle subtended by the collimator, $\pm 0.8$ mrad, was a significant fraction of the smaller $\theta_p$.

The acceptance for T1 was insensitive to these effects and was determined by a Monte Carlo calculation. Comparison of the raw momentum distributions at positive and negative values of the same $\theta_p$ gave further evidence that the T1 acceptance was independent of $\theta_p$. The acceptances for T2 and T3 were determined from the experimentally determined ratios to T1. The acceptance for T3 was independent of $\theta_p$, but that for T2 showed a significant variation with the sign of $\theta_p$ for its lower values at momenta below 150 GeV. This is illustrated for $\pm 10$ mrad in Fig. 3.

In the polarization analysis, it was assumed that the electronic efficiency of the triggers was, on average, the same for the total samples of data taken at positive and negative values of each production angle. Thus, it canceled in the analysis described in Sec. IV. In order to minimize the effects of time variations of this efficiency, the production angles were reversed at intervals of several hours over the duration of the run.

## III. EVENT SELECTION

In event selection and all subsequent analysis, the procedures, the computer programs, and the calibration constants were identical for positive and negative production angles in order to avoid introducing effects which would produce biases in the polarization calculation.

Triggers were analyzed off-line for a $V$ topology, i.e., a positive and negative track originating from a common vertex within the fiducial boundaries of the decay volume. For production angles less than 10 mrad, at least 60% of the raw triggers satisfied this criterion. This decreased at larger production angles to 26% at 20 mrad. The major effect was the decrease in the rates of $\Lambda$, $\bar{\Lambda}$, and $K_S^0$ relative to backgrounds from neutron and gamma interactions in the apparatus.

For reconstructed tracks, the momenta of the two particles were calculated as well as the $(p\pi^-)$, $(\pi^+\pi^-)$, and $(\bar{p}\pi^+)$ invariant masses. For each event an uncertainty in the mass, $\sigma_m$, was determined based on uncertainties in the momentum determination of the charged tracks and the reconstructed vertex. An event was identified as a $\Lambda$, $\bar{\Lambda}$, or $K_S^0$ if the reconstructed mass was $<3\sigma_m$ away from the known mass. If the event was identified as a $\Lambda$ it was kept in the sample as a $\Lambda$ regardless of the other mass hypotheses. If the event satisfied both $\bar{\Lambda}$ and $K_S^0$ hypotheses it was rejected from both these categories.

Events were required to pass two additional cuts. First, the reconstructed vertex was required to be, within uncertainties determined for each event, between the location of $S_1$ and $C_1$. Second, the momentum vector of the neutral parent was required to project back to within a radius of 6.4 mm of the center of the 4.8-mm-radius production target. The purpose of this requirement was to reduce the contamination in the sample of the daughter $\Lambda$'s resulting from the decay $\Xi^0 \to \Lambda\pi^0$, as well as nontarget produced $\Lambda$'s. Residual backgrounds from these sources were estimated by interpolation from the measured numbers of $\Lambda$'s outside the 6.4-mm target cut. An additional background arises from $K_S^0 \to \pi^+\pi^-$ decays with ambiguous invariant masses, i.e., the daughter tracks also satisfy the hypothesis $\Lambda \to p\pi^-$. Residual $K_S^0$ backgrounds were estimated by interpolating the distribution of unambiguous $K_S^0$'s inside the $\Lambda$ mass cut. Both of these backgrounds vary with the $\Lambda$ momentum. At 6 mrad, the worst case, this is illustrated as follows: the $\Xi^0$ background decreased from 1.5% at $p_\Lambda = 85$ GeV/$c$ to 0.5% at 125 GeV/$c$. The background from $K_S^0$ decreased from 1.3% at $p_\Lambda = 85$ GeV/$c$ to 0.8% at 165 GeV/$c$. At these levels no corrections were necessary at any production angle.

The efficiency of the software for reconstructing events, under ideal circumstances, i.e., the "perfect" Monte Carlo simulation, was 98.5% averaged over momentum. The actual efficiency was reduced by effects such as dead time, multiple Coulomb scattering, daughter-pion decays in flight, detector inefficiencies, and field irregularities in the analysis magnet. Experimental measurements and Monte Carlo studies with all known properties of the detector, including rate-dependent inefficiencies, have been used to understand these effects. (See Ref. 28 for details.) Under low-flux (small-$\theta_p$) conditions, the reconstruction efficiency rose sharply from 77% for 60-GeV $\Lambda$'s to a peak of 94% at 100 GeV and declines gradually to about 88% at 300 GeV. Under higher-flux conditions the efficiency was lower, e.g., by about 8% at 20 mrad.

These rather detailed studies give us some confidence that we understand the behavior of the apparatus and reconstruction programs when the production angle is reversed. There may be systematic uncertainties in our es-

timates of the acceptance and reconstruction efficiency of order a few percent with an even small uncertainty in the dependence on $\theta_p$. These effects contribute mainly to a quantity called a bias (Sec. IV), and their contribution to the systematic uncertainty in the polarization is negligible compared to statistical uncertainties. This is supported by the checks on systematic effects described in Sec. VII.

## IV. POLARIZATION ANALYSIS: METHOD

The polarization of the Λ ($\bar{\Lambda}$) was determined from the asymmetry in the distribution of the decay proton (antiproton). In the parent center of mass this is given by

$$dN/d\cos\theta_i = A(\cos\theta_i)(1+\alpha_\Lambda P_i \cos\theta_i) , \tag{6}$$

where $i=x,y,z$. The number of events in each bin of $\cos\theta_i$ is expected to be a linear function of $\cos\theta_i$, with a slope given by $\alpha_\Lambda P_i$, modified by $A(\cos\theta_i)$, the acceptance of the apparatus and software. This modified function of $\cos\theta_i$ is fit to each set of data where a data set is defined by a production angle. Each sign of the angle is fit independently. The technique used to fit the data, the hybrid Monte Carlo method, has been described elsewhere.[29]

The fits of the angular distributions of the daughter protons in the Λ rest system yield asymmetries which are the sum of the real polarization as well as systematic biases arising from such things as reconstruction inefficiencies that are not simulated by the hybrid Monte Carlo method. Reversal of the production angle changes the sign of the real polarization, while apparatus or software induced asymmetries are unaffected. Hence, subtraction of the asymmetries taken at equal and opposite production angles yield a bias-free polarization measurement, while the sum of the asymmetries gives a measurement of the bias. This can be summarized in the following equations in which $R_{u\pm}$ represent the raw measured asymmetries at positive and negative production angles in the direction $u=x,y,z$; $B_u$ represents the apparatus and analysis bias, and $P_u$ represents the polarization

$$\begin{aligned} R_{u\pm} &= B_u \pm P_u , \\ B_u &= \frac{R_{u+}+R_{u-}}{2} , \\ P_u &= \frac{R_{u+}-R_{u-}}{2} . \end{aligned} \tag{7}$$

A first-pass analysis with the method above yielded the three components of the polarization downstream of the magnetic beam channel for each momentum bin and production angle. $P_x$ was consistent with zero as expected from parity conservation in the production process and the fact that the precession of the spin in the beam channel occurs in the $y$-$z$ plane. The values of $P_y$ and $P_z$ were used to compute the polarization vector at the production target by using a precession angle $\phi_\pm$, which can be calculated from sign and magnitude of the precession field integral and the known magnetic moment of the Λ (Ref. 17). The production polarization was found to be consistent with no $z$ component as required by parity conservation.

A second-pass analysis did a simultaneous fit to the data imposing the constraints of parity conservation at production, and precession in the $y$-$z$ plane by the angle, $\phi_\pm$, for all momenta and production angles. The parameters of the fitting procedure were $B_{yi}$ and $B_{zi}$, the momentum-dependent biases, $P_i$ the momentum-dependent production polarization, assumed along the $y$ axis, $\int B\,dl$ in Eq. (1) for $\phi_\pm$, which was allowed to vary because, in this experiment, it had a measurement accuracy and setting precision of about 1% which is less precise than that for Refs. 17 and 18. The value of $(\mu_\Lambda/\mu_N)$ used for this analysis was $-0.6138$. These parameters were varied to minimize the function

$$\chi^2 = \sum_{i,j,k} \frac{[R_{yijk}-(B_{yi}\pm P_i\cos\phi_k)]^2}{\sigma^2_{yijk}} + \sum_{i,j,k} \frac{[R_{zijk}-(B_{zi}\pm P_i\sin\phi_k)]^2}{\sigma^2_{zijk}} . \tag{8}$$

The indices $i,j,k$ correspond, respectively, to the momentum bin, the two signs of the production angle and the two signs of the precession field. This procedure was carried out for individual magnitudes of the production angle and yielded values for the $\int B\,dl$ consistent with the measurement accuracy and setting precision of 1%.

## V. POLARIZATION RESULTS: Λ

Tables I–III give the values of the polarization $P_y$ at the production target. Figure 4 shows the subset for Λ production from Be. The data were obtained from the measured $\mathbf{P}_\Lambda$ in the decay volume and the known preces-

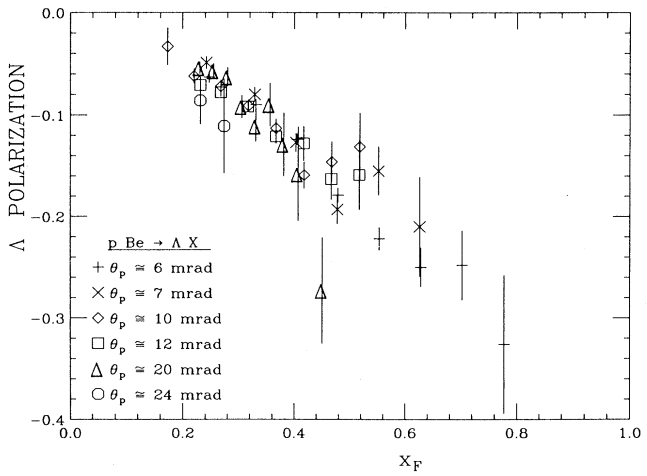


FIG. 4. The Λ polarization is shown as a function of $x_F$ for all production angles. Over this range of production angles and within experimental uncertainties, the polarization is angle (or $p_T$) independent.

sion in M1 as discussed in Sec. IV. Results are given for Be, Cu, and Pb as functions of production angle $\theta_p$ and the bin-averaged momentum, $p_\Lambda$ (Ref. 30). The corresponding average values of $x_F$ and $p_T$ are also given. Note that $\theta_p$ is not the nominal production angle, but rather an average value computed for each momentum bin from the reconstructed distributions at the production target.

The data show that at $p_T \approx 1$ GeV/$c$ the monotonic increase with $p_T$ ends and the polarization reaches a plateau in the kinematic range covered by the data. The effect is easily seen in Figs. 5(a)–5(d) where the polarization is plotted as a function of $p_T$ for subsets of the data in limited ranges of $x_F$. The kinematic behavior of the production can be described by the function

$$P_y = (C_1 x_F + C_2 x_F^3)(1 - e^{C_3 p_T^2}) . \quad (9)$$

This function was used to fit the data from this experiment and yielded a reasonable result with $\chi^2/N_{\rm DF} = 65.0/37$ and $C_3 = -4.7 \pm 1.0$ (GeV/$c$)$^{-2}$ from a standard fitting program, where $N_{\rm DF}$ is the number of degrees of freedom. However, there is relatively little data at low $p_T$, and $\chi^2$ is a highly asymmetric function of $C_3$, e.g., $\chi^2$ ($C_3 = -100.0$) = 69.1, little different from the

TABLE I. Λ polarization in $p + \mathrm{Be} \to \Lambda + X$.

| $p_\Lambda$ (GeV/$c$) | $\theta_p$ (mrad) | $p_T$ (GeV/$c$) | $x_F$ | $P_y$ at production |
|---|---|---|---|---|
| 101.3 | 6.13 | 0.621 | 0.247 | −0.063±0.004 |
| 134.3 | 6.00 | 0.806 | 0.331 | −0.090±0.004 |
| 163.5 | 5.84 | 0.955 | 0.405 | −0.124±0.005 |
| 193.0 | 5.73 | 1.106 | 0.479 | −0.179±0.007 |
| 222.5 | 5.63 | 1.253 | 0.553 | −0.222±0.011 |
| 252.1 | 5.54 | 1.397 | 0.628 | −0.250±0.019 |
| 281.9 | 5.42 | 1.528 | 0.702 | −0.248±0.034 |
| 311.8 | 5.43 | 1.693 | 0.777 | −0.326±0.068 |
| 99.6 | 7.51 | 0.748 | 0.242 | −0.049±0.006 |
| 133.7 | 7.35 | 0.983 | 0.329 | −0.080±0.007 |
| 162.9 | 7.15 | 1.165 | 0.403 | −0.127±0.009 |
| 192.5 | 7.05 | 1.357 | 0.478 | −0.193±0.014 |
| 221.8 | 6.98 | 1.548 | 0.552 | −0.155±0.024 |
| 251.4 | 6.92 | 1.740 | 0.626 | −0.210±0.049 |
| 72.9 | 10.12 | 0.738 | 0.173 | −0.033±0.018 |
| 91.0 | 9.99 | 0.909 | 0.220 | −0.062±0.007 |
| 109.7 | 9.79 | 1.074 | 0.268 | −0.072±0.006 |
| 129.1 | 9.70 | 1.252 | 0.318 | −0.091±0.006 |
| 148.7 | 9.63 | 1.432 | 0.367 | −0.113±0.009 |
| 168.6 | 9.59 | 1.617 | 0.418 | −0.159±0.013 |
| 188.5 | 9.54 | 1.798 | 0.468 | −0.146±0.020 |
| 208.5 | 9.50 | 1.981 | 0.518 | −0.131±0.033 |
| 95.2 | 11.93 | 1.136 | 0.231 | −0.071±0.006 |
| 109.5 | 11.87 | 1.300 | 0.268 | −0.078±0.004 |
| 128.7 | 11.77 | 1.515 | 0.317 | −0.092±0.005 |
| 148.4 | 11.72 | 1.739 | 0.367 | −0.121±0.007 |
| 168.3 | 11.65 | 1.961 | 0.417 | −0.128±0.017 |
| 188.2 | 11.60 | 2.183 | 0.467 | −0.163±0.020 |
| 208.1 | 11.58 | 2.410 | 0.517 | −0.159±0.034 |
| 94.9 | 20.30 | 1.926 | 0.230 | −0.054±0.006 |
| 104.6 | 20.26 | 2.119 | 0.255 | −0.057±0.007 |
| 114.5 | 20.20 | 2.313 | 0.280 | −0.063±0.009 |
| 124.5 | 20.19 | 2.514 | 0.306 | −0.092±0.011 |
| 134.4 | 20.13 | 2.705 | 0.331 | −0.111±0.015 |
| 144.4 | 20.12 | 2.905 | 0.356 | −0.090±0.021 |
| 154.3 | 20.05 | 3.094 | 0.381 | −0.129±0.031 |
| 164.4 | 20.14 | 3.311 | 0.407 | −0.158±0.046 |
| 182.0 | 20.02 | 3.644 | 0.451 | −0.273±0.052 |
| 95.2 | 23.90 | 2.275 | 0.231 | −0.086±0.023 |
| 112.0 | 23.80 | 2.666 | 0.274 | −0.111±0.046 |

TABLE II. Λ polarization in $p + \mathrm{Cu} \to \Lambda + X$.

| $p_\Lambda$ (GeV/$c$) | $\theta_p$ (mrad) | $p_T$ (GeV/$c$) | $x_F$ | $P_y$ at production |
|---|---|---|---|---|
| 116.0 | 7.42 | 0.861 | 0.284 | −0.078±0.022 |
| 176.1 | 7.13 | 1.256 | 0.437 | −0.090±0.040 |
| 90.9 | 9.96 | 0.905 | 0.220 | 0.021±0.042 |
| 109.5 | 9.76 | 1.069 | 0.268 | −0.050±0.029 |
| 128.7 | 9.67 | 1.245 | 0.317 | −0.074±0.031 |
| 148.8 | 9.60 | 1.428 | 0.368 | −0.061±0.040 |
| 90.8 | 11.92 | 1.082 | 0.220 | −0.063±0.022 |
| 108.6 | 11.85 | 1.287 | 0.265 | −0.037±0.022 |
| 128.5 | 11.70 | 1.503 | 0.316 | −0.096±0.026 |
| 148.6 | 11.66 | 1.733 | 0.367 | −0.172±0.042 |
| 168.4 | 11.59 | 1.952 | 0.417 | −0.089±0.064 |
| 90.4 | 20.32 | 1.837 | 0.219 | −0.039±0.016 |
| 108.3 | 20.25 | 2.193 | 0.265 | −0.076±0.013 |
| 128.2 | 20.18 | 2.587 | 0.315 | −0.038±0.022 |

TABLE III. Λ polarization in $p + \mathrm{Pb} \to \Lambda + X$.

| $p_\Lambda$ (GeV/$c$) | $\theta_p$ (mrad) | $p_T$ (GeV/$c$) | $x_F$ | $P_y$ at production |
|---|---|---|---|---|
| 115.8 | 7.44 | 0.862 | 0.284 | −0.052±0.022 |
| 176.0 | 7.16 | 1.260 | 0.436 | −0.088±0.088 |
| 90.7 | 9.97 | 0.904 | 0.219 | −0.040±0.033 |
| 109.3 | 9.75 | 1.066 | 0.267 | −0.073±0.029 |
| 128.5 | 9.65 | 1.240 | 0.316 | −0.093±0.033 |
| 148.8 | 9.59 | 1.427 | 0.368 | −0.067±0.040 |
| 90.7 | 11.91 | 1.080 | 0.219 | −0.051±0.022 |
| 108.5 | 11.83 | 1.284 | 0.265 | −0.054±0.022 |
| 128.9 | 11.69 | 1.507 | 0.317 | −0.059±0.024 |
| 148.7 | 11.65 | 1.732 | 0.367 | −0.061±0.035 |
| 168.5 | 11.61 | 1.956 | 0.417 | −0.125±0.058 |
| 90.4 | 20.33 | 1.838 | 0.219 | −0.043±0.033 |
| 108.6 | 20.23 | 2.197 | 0.265 | −0.051±0.041 |
| 128.3 | 20.20 | 2.592 | 0.316 | −0.123±0.059 |

minimum, while $\chi^2(C_3=-2.17)=105$ (an increase of one unit per data point) and increases dramatically for smaller negative values of $C_3$. This is easily understood. For large, negative $C_3$ the $p_T$ dependence in Eq. (9) at fiixed $x_F$ is constant and agrees reasonably well with the data, most of which are in the plateau region. (See Fig. 4.) For small, negative $C_3$, the $p_T$ dependence behaves like $p_T^2$ at fixed $x_F$ and fits the data poorly.

In order to constrain the fit better at low $p_T$, we added data from Refs. 3 and 23. Both these experiments were performed with 400-GeV protons on a Be target. $C_1$ changed by 7%, $C_2$ by 18% (in the direction to compensate for the change in $C_1$) and $C_3$ by 4%. The dependence of $\chi^2$ on the parameters was nearly symmetric. The results of this fit are $C_1=-0.268\pm0.003$, $C_2=-0.338\pm0.015$, and $C_3=-4.5\pm0.6$ $(\mathrm{GeV}/c)^{-2}$, with $\chi^2/N_{\mathrm{DF}}=109.4/69$. The form of Eq. (9) is clearly not uniquely determined by the data but it represents the data well. This fit is shown in Fig. 5.

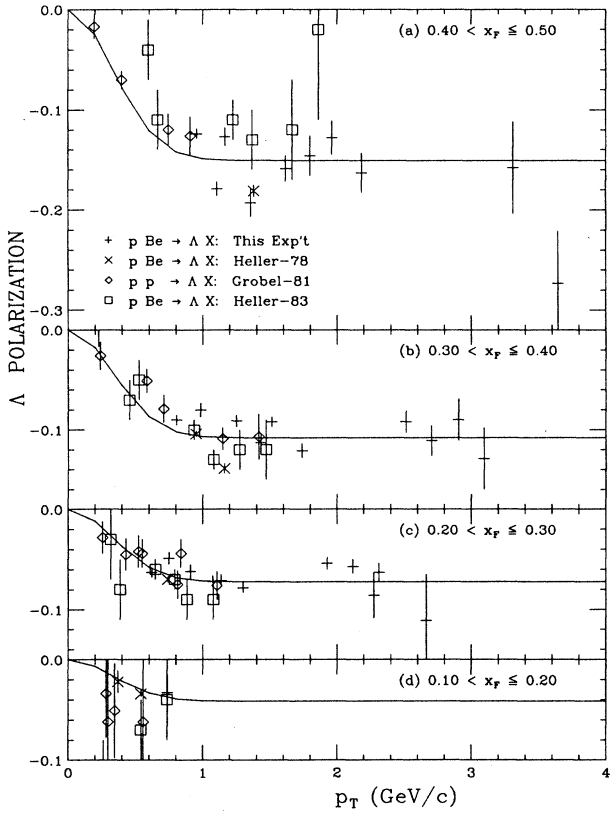


FIG. 5. Inclusive Λ polarization as a function of $p_T$ with $x_F$ restricted to each of the four ranges indicated in (a)–(d). The data plotted are from this experiment and Refs. 3, 23, and 24. All four experiments used the same spectrometer and measurement techniques. Errors when not shown are smaller than the points. The lines are a fit to the $p$ + Be data using Eq. (9). Note that some of the scatter in the points is due to differences in the values of $x_F$ at which they were measured.

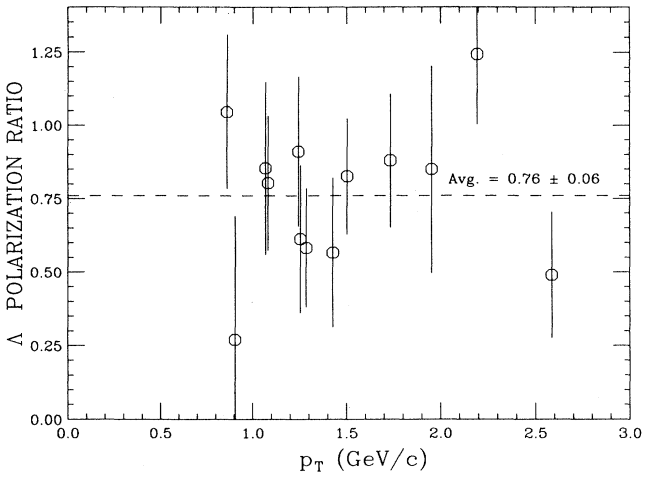


FIG. 6. The ratio of the momentum-averaged copper and lead polarization to the polarization from beryllium is shown. Note that the copper and lead data are combined to improve the statistical power in measuring the nuclear effect.

Alternate functions of $p_T$ were considered while maintaining the $x_F$ dependence of Eq. (9). A constant, while it represents the data of this experiment well, is clearly inconsistent with the other experiments and with the requirement that the polarization be zero at $p_T=0$. A factor linear in $p_T$ is the simplest function which satisfies this latter requirement: i.e.,

$$P_y=(C_1x_F+C_2x_F^3)p_T\ . \tag{10}$$

It was tried and $\chi^2/N_{\mathrm{DF}}$ increased to 682/38 for the data of this experiment, and to 982/69 for the combined data of the three experiments.

Some additional evidence for the flattening of the polarization above $p_T=1$ GeV/$c$ can be obtained from the data of Ref. 24 in which Λ's were produced by 400-GeV protons on a hydrogen target. A fit to Eq. (9) yields $\chi^2/N_{\mathrm{DF}}=42.6/48$, while that for Eq. (10) yields $\chi^2/N_{\mathrm{DF}}=60.7/49$. While both are reasonable fits in absolute "goodness of fit," the change suggests that the linear function is significantly poorer.

The dependence of the Λ polarization on production target material has been measured by several experiments.[6,24–26] All experiments agree that the magnitude of the polarization decreases with increasing atomic number. For the present experiment the ratio of the polarization of Cu and Pb (combined data) to Be averaged over the momentum range 85–200 GeV/$c$ is $0.76\pm0.06$. The data are shown as a function of $p_T$ in Fig. 6. There is no evidence that the ratio varies with $p_T$ at the present level of statistical accuracy.

## VI. POLARIZATION RESULTS: $\bar{\Lambda}$

Previous measurements have shown a null result to a precision of 0.02 in $P_{\bar{\Lambda}}$ up to a transverse momentum of 0.95 GeV/$c$ (Ref. 3). The present experiment, with a

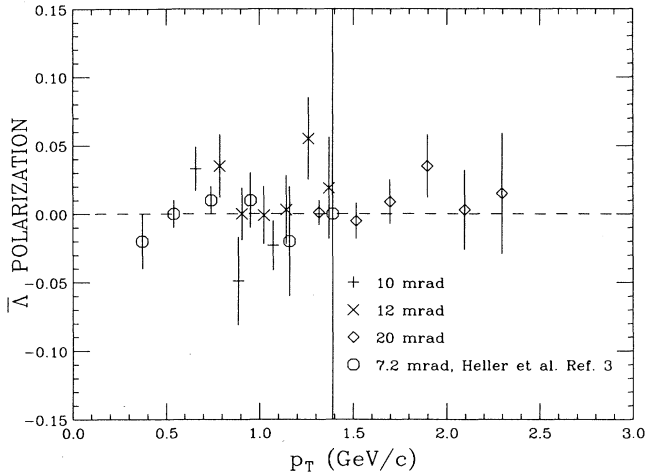


FIG. 7. The polarization results for the $\bar{\Lambda}$ samples are shown at 10, 12, and 20 mrad. The polarization is consistent with zero up to a transverse momentum of 2.3 GeV/$c$.

sample of 788 327 events, extends the measurement up to $p_T=2.3$ GeV/$c$, as shown in Fig. 7 and in Table IV (Ref. 31). The global average over momentum and production angle ($\langle p_T\rangle=1.2$ GeV/$c$, $\langle x_F\rangle=0.16$) is $P_{\bar{\Lambda}}=+0.006\pm0.005$. For comparison, at the same $x_F$ and $p_T$, Eq. (9) gives $P_\Lambda=-0.026\pm0.002$.

## VII. BIASES AND SYSTEMATIC ERRORS

The calculation described in Sec. IV is directed toward a simultaneous measurement of two things: the biases (a property of the experimental apparatus) and the polarization (the physics goal of the experiment). The frequent reversal of production angle (and, thus, polarization) yields two data sets which are symmetric in the bias and antisymmetric in the polarization. Because of the opposite symmetry, precise measurements of polarization can be achieved even in the presence of the significant biases shown in Fig. 8.

A small contribution to the bias in each measurement arises from lack of exact equality ($\leq 0.5$ mrad) in the "matched" positive and negative values of the nominal production angles. This arises from alignment and statistical fluctuations in the way the events populate beam phase space. Similar fluctuations occur in the momenta in a given momentum bin. In general the magnitudes of the matched positive and negative polarization values will differ because of these differences in kinematic quantitiies, and the difference appears as part of the bias. The magnitude of the polarization obtained from our analysis is the weighted average of the polarization magnitudes of the two samples. The angle and momentum reported for each bin are similarly weighted. Systematic errors arising from this procedure are small compared to the statistical uncertainties.

The main contributions to the biases are apparatus

TABLE IV. $\bar{\Lambda}$ polarization in $p+\mathrm{Be}\rightarrow\bar{\Lambda}+X$.

| $p_\Lambda$ (GeV/$c$) | $\theta_p$ (mrad) | $p_T$ (GeV/$c$) | $x_F$ | $P_y$ at production |
|---|---|---|---|---|
| 65 | 10.11 | 0.657 | 0.152 | 0.033±0.016 |
| 89 | 9.96 | 0.886 | 0.215 | −0.049±0.032 |
| 108 | 9.93 | 1.072 | 0.264 | −0.023±0.018 |
| 65 | 12.11 | 0.787 | 0.152 | 0.035±0.023 |
| 75 | 12.07 | 0.905 | 0.179 | 0.000±0.019 |
| 85 | 12.04 | 1.023 | 0.205 | −0.001±0.021 |
| 95 | 12.02 | 1.142 | 0.231 | 0.003±0.025 |
| 105 | 12.00 | 1.260 | 0.256 | 0.055±0.030 |
| 115 | 11.97 | 1.377 | 0.282 | 0.019±0.037 |
| 65 | 20.24 | 1.316 | 0.152 | 0.001±0.009 |
| 75 | 20.21 | 1.516 | 0.179 | −0.005±0.013 |
| 84 | 20.19 | 1.696 | 0.202 | 0.009±0.016 |
| 94 | 20.17 | 1.896 | 0.228 | 0.035±0.023 |
| 104 | 20.15 | 2.096 | 0.254 | 0.003±0.029 |
| 114 | 20.15 | 2.297 | 0.279 | 0.015±0.044 |

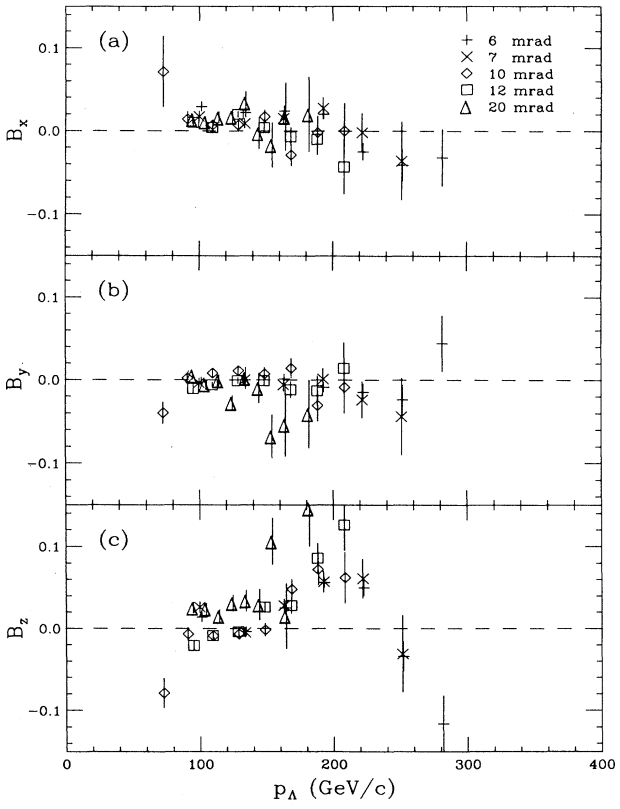


FIG. 8. The measured biases along each of the coordinate axes are shown as functions of momentum: (a) $B_x$, (b) $B_y$, and (c) $B_z$. Except for the 20-mrad data, the biases show no significant dependence on production angle.

effects not well reproduced by the hybrid Monte Carlo programs. They represent our lack of complete understanding of the apparatus, and must be measured. The reliability of our techniques for measuring biases and polarizations has been verified by a set of highly redundant tests and cross-checks performed in an earlier experiment. These are reported briefly in Ref. 17 and in great detail in Ref. 32. Some of these checks were repeated in the present experiment and are described in the following paragraphs.

The biases are insensitive to production angle as expected, and they tend to be small for the $x$ and $y$ directions where the apparatus is reasonably symmetric.

Under the assumption that parity is conserved in the interaction, the $x$ component of the polarization must be zero. The deviation of $P_{x\Lambda}$ from zero is an indication of a bias originating in the apparatus or analysis which is not corrected by our procedures. In this experiment $P_{x\Lambda}<0.003\pm0.001$ for all production angles less than 20 mrad, and at 20 mrad $P_{x\Lambda}=+0.009\pm0.002$. These results are momentum averaged and momentum independent within statistical uncertainties.

A second check on systematics was done by measuring the asymmetries in the decay $K_S^0\to\pi^+\pi^-$. This was done for data at 6 and 20 mrad. At 6 mrad, all components of the measured asymmetry were $\leq0.006\pm0.010$ in magnitude. At 20 mrad they were $\leq0.011\pm0.014$.

The conclusion to be drawn from the study of systematic effects is that at angles below 20 mrad the systematic errors are negligible. At 20 and 24 mrad we assign a systematic uncertainty of $\pm0.01$ to the polarization results based on the measurements described in the preceding paragraphs. Additional justification for larger systematic uncertainties at the highest angles comes from the behavior of the biases shown in Fig. 8. We have been able to think of only one mechanism to explain the behavior at higher angles which fits the properties of the apparatus and running conditions. At the beam intensities used for 20 and 24 mrad, the large flux of charged particles in our apparatus from decays and neutral particle interactions may have caused dead-time inefficiencies and acceptance losses in the proportional chambers which deviated from the Monte Carlo programs. This may be responsible for the large-angle behavior of the biases which differ from those at small angle by up to several percent. It is not unlikely that the effect differed for positive and negative production angles by a significant fraction of its value. This is consistent with the observed 1% deviations from expected zero asymmetries, and supports our assignment of a larger systematic uncertainty at these angles.

A sample of unpolarized Monte Carlo events generated with known appratus inefficiencies were analyzed by the same techniques as the data. The asymmetries, which arise wholly from reconstruction biases, yield $B_x=-0.003\pm0.012$, $B_y=0.009\pm0.012$, and $B_z=0.019\pm0.013$, in reasonable agreement with the biases measured from data.

A final item to consider in the discussion of systematic effects is the dilution of the Λ polarization resulting from contamination of the sample by the daughter Λ's from $\Sigma^0\to\Lambda\gamma$ and $\Sigma^*\to\Lambda\pi$. There are no data in our energy range on these processes to unfold the effects of the daughter-Λ polarization from our measured polarization. However, a crude estimate of the size of the effect can be made on the basis of related measurements. For simplicity we discuss this mainly in terms of the $\Sigma^0$ as the single source of the daughter Λ's. Three ingredients enter the discussion.

(1) We assume that the parent-$\Sigma^0$ polarization is $\mathbf{P}_\Sigma\approx-\mathbf{P}_\Lambda$. This assumption is supported by polarization measurements of $\Sigma^+$(Ref. 9) and $\Sigma^-$ (Ref. 11) at Fermilab, and $\Sigma^0$ (Ref. 33) at Brookhaven. (2) The daughter-Λ polarization can be represented as $\mathbf{P}_d=f\mathbf{P}_\Sigma$, where $-1<f<+1$. For $\Sigma^0\to\Lambda\gamma$ averaged over all decay angles relative to the polar axis, $\mathbf{P}_\Sigma,\mathbf{P}_d=-\frac{1}{3}\mathbf{P}_\Sigma$, i.e., $f=-\frac{1}{3}$ (Ref. 34). For a subsample of the daughters in the equatorial plane, $f=0$. Since the polarization direction is perpendicular to the beam direction, the daughter-Λ polarization must lie between these two extremes. The half angle of the beam channel collimator is 0.8 mrad. For most of our data, this is larger than the angle between the daughter Λ momentum and the parent $\Sigma^0$ momentum. There is full acceptance for Λ's from $\Sigma^0$'s aimed directly along the collimator axis. For off-axis Σ's our collimator tend to sample all decay angles approximately uniformly. Thus, the first case, $\mathbf{P}_d=-\frac{1}{3}\mathbf{P}_\Sigma$ is favored for $\Sigma^0\to\Lambda\gamma$. (For $\Sigma^*$ decays, the decay angle is triple or more that of $\Sigma^0$, and the daughter-Λ average polarization is closer to zero.) (3) The fraction of the daughter Λ's in the beam is represented by $\beta$. References 35 and 36 have determined the fraction of the daughter Λ's from $\Sigma^0$ at Brookhaven energies to be $0.278\pm0.011\pm0.05$ for 28.5-GeV protons on Beryllium. No other data exist from which to estimate $\beta$ at Fermilab energies.

This allows us to write down the measured polarization in terms of the polarization for directly produced Λ's:

$$\begin{aligned}\mathbf{P}_\Lambda&=(1-\beta)\mathbf{P}_\Lambda^{\text{direct}}+\beta f\mathbf{P}_\Sigma\\&\approx\mathbf{P}_\Lambda^{\text{direct}}(1-\beta-f\beta)\\&\approx\mathbf{P}_\Lambda^{\text{direct}}(1-\beta)\quad(f=0)\\&\approx\mathbf{P}_\Lambda^{\text{direct}}(1-\tfrac{2}{3}\beta)\quad(f=-\tfrac{1}{3})\,.\end{aligned}\tag{11}$$

The measured polarization is diluted from that of directly produced Λ's by a factor depending on the relative production cross sections and on $x_F$ since the mean momentum of the daughters will be lower than the mean momentum of the directly produced Λ's. If we neglect this kinematic effect, and assume $\beta=0.3$ then the dilution is between 20% and 30%.

## VIII. CONCLUSIONS

It is apparent that one can associate polarization with the production mechanism of the hyperon. The $\bar{\Lambda}$, with no constituents in common with the incident particle, has no measurable polarization. All of its quarks have to be created in the interaction; hence, the dynamics of forming the final state is symmetric with regard to any of its

valence quarks. The $\Lambda$, however, exhibits a leading particle behavior in proton-nucleon interactions: $d\sigma/dx_F \sim(1-x_F)^n$, where $n\approx 1$ for forward production.[37,38] This arises from the fact that the $\Lambda$ shares two quarks with the incident proton.

For the kinematic limits $x_F\rightarrow 0$ and $x_F\rightarrow 1$ one can make simple assertions about the behavior of $P_\Lambda$. In the former case the fact that the $\bar{\Lambda}$ differential cross section extrapolated to $x_F=0$ differs little from the corresponding $\Lambda$ cross section is suggestive that their production mechanisms are not different for central production (diquark states are unlikely). Then $P_\Lambda(x_F=0)\simeq P_{\bar{\Lambda}}(x_F=0)\simeq 0$.

The above conclusion is somewhat supported by another argument. The condition $P_\Lambda(x_F=0)=0$ is an absolute requirement, based on rotational invariance, for the $\Lambda$'s produced in $pp\rightarrow\Lambda X$ on protons in the target nucleus. Isotopic spin invariance then imposes a similar condition on the $I=1$ production of $\Lambda$'s from target neutrons. Since this argument cannot be extended to the $I=0$ part of the production, it is not absolute. Nevertheless, unless there is some compensating enhancement of the polarization in $I=0$ production, it suggests that the polarization is suppressed at $x_F=0$. The choice of odd powers of $x_F$ in the function used in Eq. (9) is guided by this.

For the case $x\approx 1$ the $\Lambda$ production must be dominated by the recombination of a $ud$ system, intact from the proton, and an $s$ quark from the interaction with the target. Since polarization implies a degree of coherence in forming the final state from the possible amplitudes, it is natural to assume that **P** is largest in the case where there are few significant ways to form the $\Lambda$. Equation (9) can be extrapolated to near the forward limit, $P_\Lambda(x_F\approx 1, p_T\geq 1)\simeq -0.5$. Estimates[35,36] of the cross-section ratio of inclusive $\Sigma^0$ to direct $\Lambda$ production suggest that $P_\Lambda^{\text{direct}}\approx -0.6$. If dilution due to higher mass strange resonances is important, the magnitude of the direct polarization could be even greater than this.

A description of hyperon polarization was proposed soon after the initial observation of $\Lambda$ polarization.[39] It involved the interference of two triple-Regge diagrams, but lacked any way of generating the nonzero relative phase required for polarization. Recently, it has been suggested that interference of different final-state resonances might provide this phase difference.[40]

Several other phenomenological models[3,41–43] have been proposed to account for the dynamical origin of inclusive polarization. They describe the process in terms of constituent quarks and have certain features in common. They all rely on a picture of baryon structure in which the $s$ quark carries all the spin information for the $\Lambda$. All involve a strong influence of valence quarks or diquarks common to the incident and outgoing baryons. This appears to be demanded by the observed relative signs of the polarization of various final-state hyperons and the lack of significant polarization in antihyperons produced by protons. All the constituent models focus on a picture in which the polarization arises not from hard scattering of partons, but from the process in which constituents, particularly spectator quarks or diquarks from the incident proton, sort out their color fields to become color-neutral final-state hadrons, i.e., the fragmentation.

The persistence of a large polarization at large $p_T$ cannot be explained in terms of a naive, low-order QCD calculation. It has been argued using basic assumptions from perturbative theory that $P_\Lambda$ must be small or zero in the "large"-$P_T$ limit.[44,45] Polarization requires an interference of complex spin-flip and nonflip amplitudes which have a significant phase difference. In lowest-order perturbative QCD, all amplitudes are relatively real. This tends to rule out polarization in the hard scattering of partons which seems to be well described in low-order QCD. The observation of undiminished polarization near 4 GeV/$c$ implies that either perturbative QCD does not apply or that another mechanism is responsible, such as interference of excited states[45,46] or the fragmentation process.

Recently, higher-order QCD calculations of $s$-$\bar{s}$ pair production by gluon fusion has been studied as a mechanism for polarizing the $s$ quark.[43] The computed $s$-quark polarization shows an $x_F$ dependence similar to that reported here, and it peaks at $p_T$ in the range 1.0–1.5 GeV/$c$, dropping slowly thereafter. However, the peak $s$-quark polarization of 5% is smaller than the $\Lambda$ polarization we observe. These authors discuss a preliminary study of mechanisms, such as those proposed in earlier models,[41] by which the polarization is enhanced when the $s$-quark combines with a spinless, valence $ud$-diquark from the incident proton to produce the observed $\Lambda$.

## ACKNOWLEDGMENTS

We wish to thank the staff of Fermilab, in particular the Meson Laboratory staff and the Computer Department, for providing much of the help and resources needed to carry out this experiment. We are especially grateful to Stan Sobczynski for the design and construction of the AVB system, crucial to this experiment, which worked splendidly. We thank George Ott, Jesse Jaske, Dan Feyma, and Carl Meulheisen for their help in preparing the detection apparatus. This work was supported in part by the U.S. Department of Energy and the National Science Foundation.

*Present address: Fermilab, P. O. Box 500, Batavia, IL 60510.
†Present address: MP-5, Los Alamos National Laboratory, P. O. Box 1663, Los Alamos, NM 87545.
‡Present address: Fonar Corporation, 110 Marcus Drive, Melville, NY 11747.
§Formerly P. C. Petersen; present address: Physics Department, Yale University, New Haven, CT 06511.
**Present address: Department of Physics, University of California, Berkeley, CA 94705.
††Present address: Philips Medical Systems, 710 Bridgeport Avenue, Shelton, CT 06484.

[1]G. Bunce *et al.*, Phys. Rev. Lett. **36**, 1113 (1976).
[2]K. Heller *et al.*, Phys. Lett. **68B**, 480 (1977).
[3]K. Heller *et al.*, Phys. Rev. Lett. **41**, 607 (1978); **45**, 1043(E)

(1980).
[4]F. Lomanno *et al.,* Rev. Lett. **43**, 1905 (1979).
[5]S. Erhan *et al.,* Phys. Lett. **82B**, 301 (1979).
[6]K. Raychaudhuri *et al.,* Phys. Lett. **90B**, 319 (1980); **93B**, 525(E) (1980).
[7]F. Abe *et al.,* Phys. Rev. Lett. **50**, 1102 (1983); J. Phys. Soc. Jpn. **52**, 4107 (1983).
[8]P. T. Cox *et al.,* Phys. Rev. Lett. **46**, 877 (1981).
[9]C. Wilkinson *et al.,* Phys. Rev. Lett. **46**, 803 (1981).
[10]C. Ankenbrandt *et al.,* Phys. Rev. Lett. **51**, 863 (1983).
[11]L. Deck *et al.,* Phys. Rev. D **28**, 1 (1983).
[12]R. Rameika *et al.,* Phys. Rev. Lett. **52**, 581 (1984).
[13]Y. W. Wah *et al.,* Phys. Rev. Lett. **55**, 2551 (1985).
[14]G. Zapalac *et al.,* Phys. Rev. Lett. **57**, 1526 (1986).
[15]P. Skubic *et al.,* Phys. Rev. D **18**, 3115 (1978).
[16]L. Pondrom, Phys. Rep. **122**, 58 (1985).
[17]L. Schachinger *et al.,* Phys. Rev. Lett. **41**, 1348 (1978).
[18]C. Wilkinson *et al.,* Phys. Rev. Lett. **58**, 855 (1987).
[19]A preliminary report of analysis in progress was given by K. Johns, in *High-Energy Spin Physics,* proceedings of the Eighth International Symposium, Minneapolis, Minnesota, 1988, edited by K. Heller (AIP Conf. Proc. No. 187) (AIP, New York, 1989), Vol. I, pp. 374–383.
[20]S. Y. Hsueh *et al.,* Phys. Rev. Lett. **54**, 2399 (1985).
[21]S. Y. Hsueh *et al.,* Phys. Rev. D **38**, 2056 (1988).
[22]N. Cabibbo, Phys. Rev. Lett. **10**, 531 (1963); N. Cabibbo and F. Chilton, Phys. Rev. **137**, B1628 (1965).
[23]K. Heller *et al.,* Phys. Rev. Lett. **51**, 2025 (1983).
[24]R. Grobel, Ph.D. thesis, University of Wisconsin, 1981.
[25]K. Heller *et al.,* Phys. Rev. D **16**, 2737 (1977).
[26]F. Abe *et al.,* Phys. Rev. D **34**, 1950 (1986).
[27]The production plane and the direction of the precession field were rotated 90° in this experiment relative to previous experiments with this apparatus, e.g., Refs. 1, 17, 8, 12, 18, and 11.
[28]B. Lundberg, Ph.D. thesis, University of Wisconsin, 1984.
[29]G. Bunce, Nucl. Instrum. Methods **172**, 553 (1980).
[30]Momentum bins for Λ were 30 GeV/$c$ wide for 6- and 7-mrad data and 20 GeV/$c$ wide for 10, 12, and 20 mrad. The two 24-mrad bins were done in transverse momentum: 2.0 GeV/$c$ $< p_T <$ 2.5 GeV/$c$ and $p_T >$ 2.5 GeV/$c$.
[31]Where sufficient data exist for $\bar{\Lambda}$ polarization, the bin widths are the same as for Λ except for 7 mrad where the two bins were 0.5 GeV/$c$ $< p_T <$ 1.0 GeV/$c$ and $p_T >$ 1.0 GeV/$c$.
[32]L. Schachinger, Ph.D. thesis, Rutgers University, 1978.
[33]E. C. Dukes *et al.,* Phys. Lett. B **193**, 135 (1987).
[34]R. Gatto, Phys. Rev. **109**, 610 (1958).
[35]M. Sullivan *et al.,* Phys. Lett. **142B**, 473 (1984).
[36]M. Sullivan *et al.,* Phys. Rev. D **36**, 674 (1987).
[37]A. Beretvas *et al.,* Phys. Rev. D **34**, 53 (1986).
[38]The measured values for $n$ are 0.86±0.04 for Be, 0.99±0.05 for Cu, and 1.06±0.03 for Pb. The cross section analysis of Ref. 28 is in excellent agreement with these numbers.
[39]T. Devlin *et al.,* Nucl. Phys. **B123**, 1 (1977).
[40]P. Cea *et al.,* Phys. Lett. B **193**, 361 (1987).
[41]T. DeGrand and H. Miettinen, Phys. Rev. D **24**, 2419 (1981).
[42]B. Andersson, G. Gustafson, and A. Ingelman, Phys. Lett. **85B**, 417 (1979).
[43]W. G. D. Dharmaratna and Gary R. Goldstein, Tufts University Report No. TH-G88-4 (unpublished); also in *High-Energy Spin Physics* (Ref. 19), Vol. I, pp. 291–294.
[44]G. Kane, J. Pumplin, and W. Repko, Phys. Rev. Lett. **41**, 1689 (1978).
[45]N. Craigie, K. Hidaka, M. Jacob, and F. Renard, Phys. Rep. **99**, 70 (1983).
[46]G. Preparata, in *High Energy Physics with Polarized Beams and Polarized Targets,* proceedings of the International Symposium, Lausanne, Switzerland, 1980, edited by C. Joseph and J. Soffer (Experimentia Supplementum, Vol. 38) (Birkhauser, Basel, 1981), p. 121.